SCIENCE CHINA PRESS

SCIENCE CHINA Chemistry
https://doi.org/10.1007/s11426-025-3327-1

BRIEF COMMUNICATIONS

Centrally-extended iridium complex enables three-dimensional non-fullerene acceptor to achieve high-performance organic photovoltaics

Ruibin Bian[1], Xiangjian Cao[1], Zhaoyang Yao[1*], Shuhui Ding[1], Wenkai Zhao[2], Yu Zhang[1], Bin Kan[2], Guankui Long[2], Chenxi Li[1], Xiangjian Wan[1*] & Yongsheng Chen[1*]

[1]State Key Laboratory and Institute of Elemento-Organic Chemistry, The Centre of Nanoscale Science and Technology and Key Laboratory of Functional Polymer Materials, Renewable Energy Conversion and Storage Center (RECAST), Frontiers Science Center for New Organic Matter, College of Chemistry, Nankai University, Tianjin 300071, China
[2]School of Materials Science and Engineering, National Institute for Advanced Materials, Renewable Energy Conversion and Storage Center (RECAST), Nankai University, Tianjin 300350, China
*Corresponding authors (email: zyao@nankai.edu.cn; xjwan@nankai.edu.cn; yschen99@nankai.edu.cn)

Received 28 November 2025; Accepted 28 January 2026; Published online 8 May 2026

1 Introduction

Organic solar cells (OSCs) have been recognized as a promising route to green energy with unique features of lightweight [1], low-cost [2,3], solution-processability [4,5], semi-transparency [6,7], and flexibility [8,9]. As one of the light-harvesting components, fullerene-based compounds have served as a pioneer for acceptors due to their high electron affinity, good processability, excellent and isotropic charge transport, *etc*. [10–14]. With the emergence of non-fullerene acceptors (NFAs), the power conversion efficiency of OSCs has surged from less than 10% to over 20% due to the broad absorption, tunable energy level and lower energy loss of NFAs [15–22]. Note that the most irreplaceable characteristics of fullerene acceptors have been inherited by NFAs except the excellent isotopic charge transport [23], rendering a strict limitation to tune the specific molecular stacking orientations of NFAs during film formation [13,24,25]. Exploring three-dimensional (3D) NFAs with fullerene-mimicking conformations may help to escape from the cumbersome operation of morphology control, by achieving two-in-one advantages of both fullerene and NFAs. However, the 3D molecular geometry of NFAs will inevitably impede their tight intermolecular stackings, making it quite challenging to construct high-performance OSCs [26–28].

To maximize the advantages of fullerene-mimicking conformation while circumventing its hindered intermolecular stacking, we proposed a new pathway to build the fullerene-conformation-mimicking NFAs in this work: extending the backbone of NFAs towards multiple directions through a 3D molecular centrally-extended center (Figure 1a). Note that both the structure of centrally-extended center [29,30] and connection type with NFA backbones [31–35] determine the molecular conformation and intermolecular packing modes significantly. Herein, two 3D centrally-extended structural cores of triptycene and octahedral chelated iridium(III) complex were delicately applied. Among them, triptycene afforded the highly rigid and symmetrical CH25 by fusing with three NFA backbones (Figure 1b) [36]. In another case, an exotic CH61 was constructed by connecting three central units of NFAs to an octahedral chelated iridium(III) complex through the single-bond. Both CH25 and CH61 exhibit the three-dimensional, propeller-like conformation with six 2-(3-oxo-2,3-dihydroinden-1-ylidene) malononitrile (INCN) terminals extending towards different directions, thus mimicking the charge transport property of fullerene-based acceptors to some extent. Due to the featured coordinate bond and single-bond connection, CH61 exhibited a relatively flexible molecular skeleton compared to that of CH25. The systematic investigation revealed that CH61 also possesses the enhanced light harvest, weaker exciton binding, more balanced hole/electron transport and suppressed non-radiative charge recombination. As a result, PM6:CH61-based binary OSC achieves an excellent efficiency of 17.85%, which not only greatly surpasses that of 3.41% for PM6:CH25 but also represents a quite rare high-performance system for a three-dimensional trimeric acceptor. Please note that although these 3D NFAs achieve a comparable electron mobility compared to the state-of-the-art acceptors (Figure S1 and Table S1, Supporting Information online), their isotropic charge transport is hard to clearly evaluate, making the relation between 3D structure and isotropic charge transport still unclear. Overall, this work demonstrates the potential for high-performance OSC systems by designing fullerene-conformation-mimicking NFAs with a two-in-one feature of both fullerene acceptors and NFAs.

2 Results and discussion

The synthesis route to CH61 and corresponding characterization analysis were illustrated in Scheme S1 (Supporting Information online) and Figures S19–S30. As revealed by density functional theory (DFT) calculations, both CH25 and CH61 possess the three-dimensional fullerene-mimicking configurations with six cantilevers extending towards different directions (Figure 1c and Figure S2). Among them, CH25 has a highly symmetrical structure (C_{3v} point group), whereas CH61 is less symmetrical due to the central iridium(III) induced facial isomers [37]. This results in a significantly larger dipole moment for CH61 (9.04 Debye) compared to CH25 (0.02 Debye). The spatial distribution of the highest occupied molecular orbitals (HOMOs) and the lowest unoccupied molecular orbitals (LUMOs) is similar for both CH25 and CH61

Citation: Bian R, Cao X, Yao Z, Ding S, Zhao W, Zhang Y, Kan B, Long G, Li C, Wan X, Chen Y. Centrally-extended iridium complex enables three-dimensional non-fullerene acceptor to achieve high-performance organic photovoltaics. *Sci China Chem*, https://doi.org/10.1007/s11426-025-3327-1

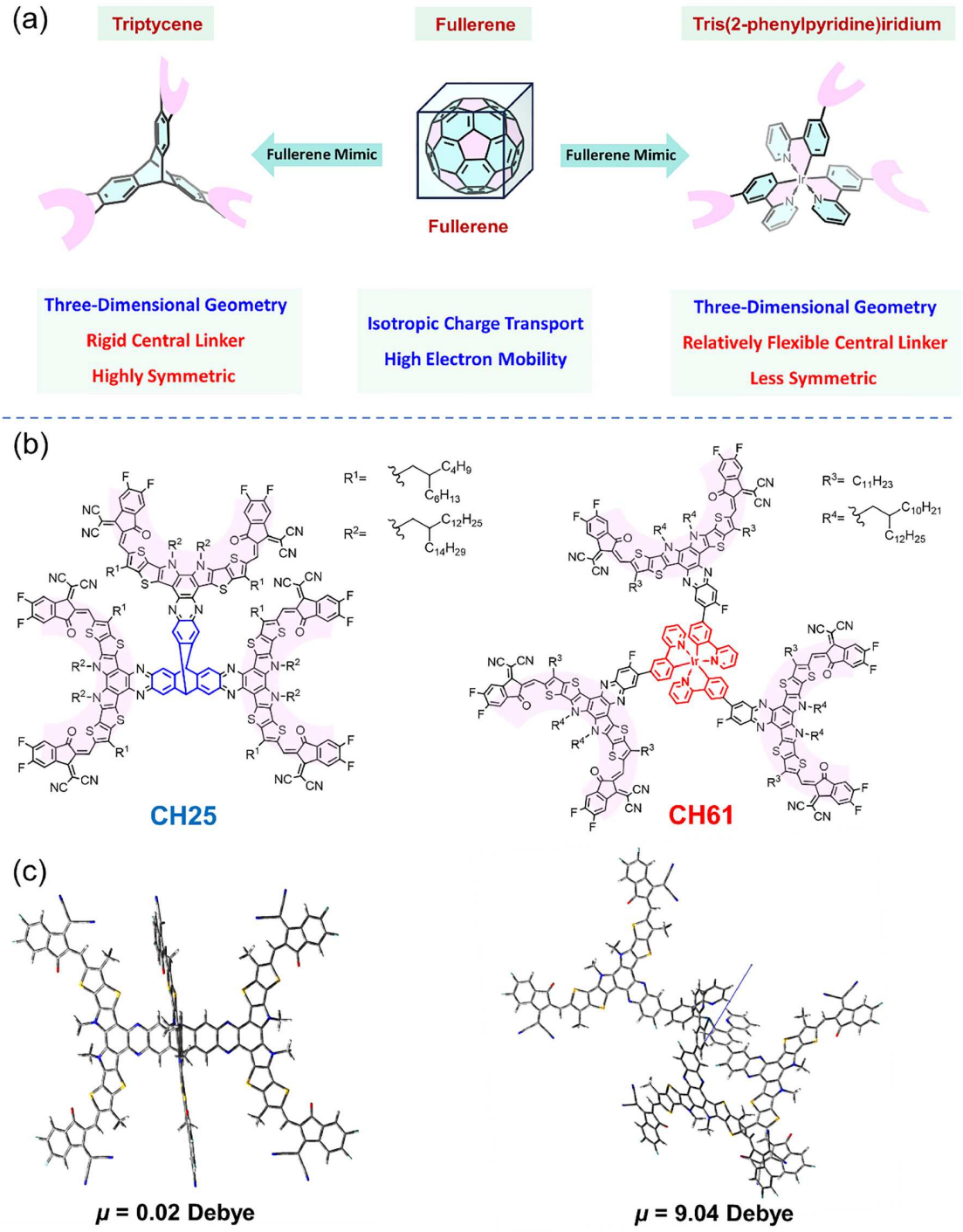

Figure 1 (Color online) (a) Molecular design of fullerene-mimicking NFAs. (b) Chemical structures of CH25 and CH61. (c) Optimized configurations and dipole moments (μ) derived from DFT calculations.

(Figure S3). The HOMOs are located on N,S-heterocycle, while the LUMOs further spread to INIC terminals with the most probability on cyano-groups. The rare distribution of frontier molecular orbitals on triptycene or tris(2-phenylpyridine)iridium manifests that the 3D centrally-extended center mainly works as an effective molecular stacking regulator rather than the chromophore. Therefore, the comparable HOMO and LUMO energy levels could be afforded by DFT calculations (Figure S3) and cyclic voltammetry (CV) measurements (Figure 2a and Figure S4).

Due to the comparable energy levels, CH25 and CH61 present similar absorption in solutions with the maximum wavelength locating at 752 and 748 nm, respectively (Figure 2b). Whereas the maximum absorption peak of CH25 only red-shifted by 46 nm from solution to film compared to that of 59 nm for CH61, suggesting the more desired molecular stackings for CH61 [38,39]. Furthermore, CH61 exhibits slightly larger molar extinction coefficients in solution and a higher maximum absorption coefficient in films compared to CH25. (Figure 2c and Figure S5). As displayed in Figure S6 and Figure 2d, CH25 does not have an obvious π-π stacking signal in the out-of-plane (OOP) direction revealed by the grazing-incidence wide-angle X-ray scattering (GIWAXS) measurements. This may result from its 3D molecular geometry and highly

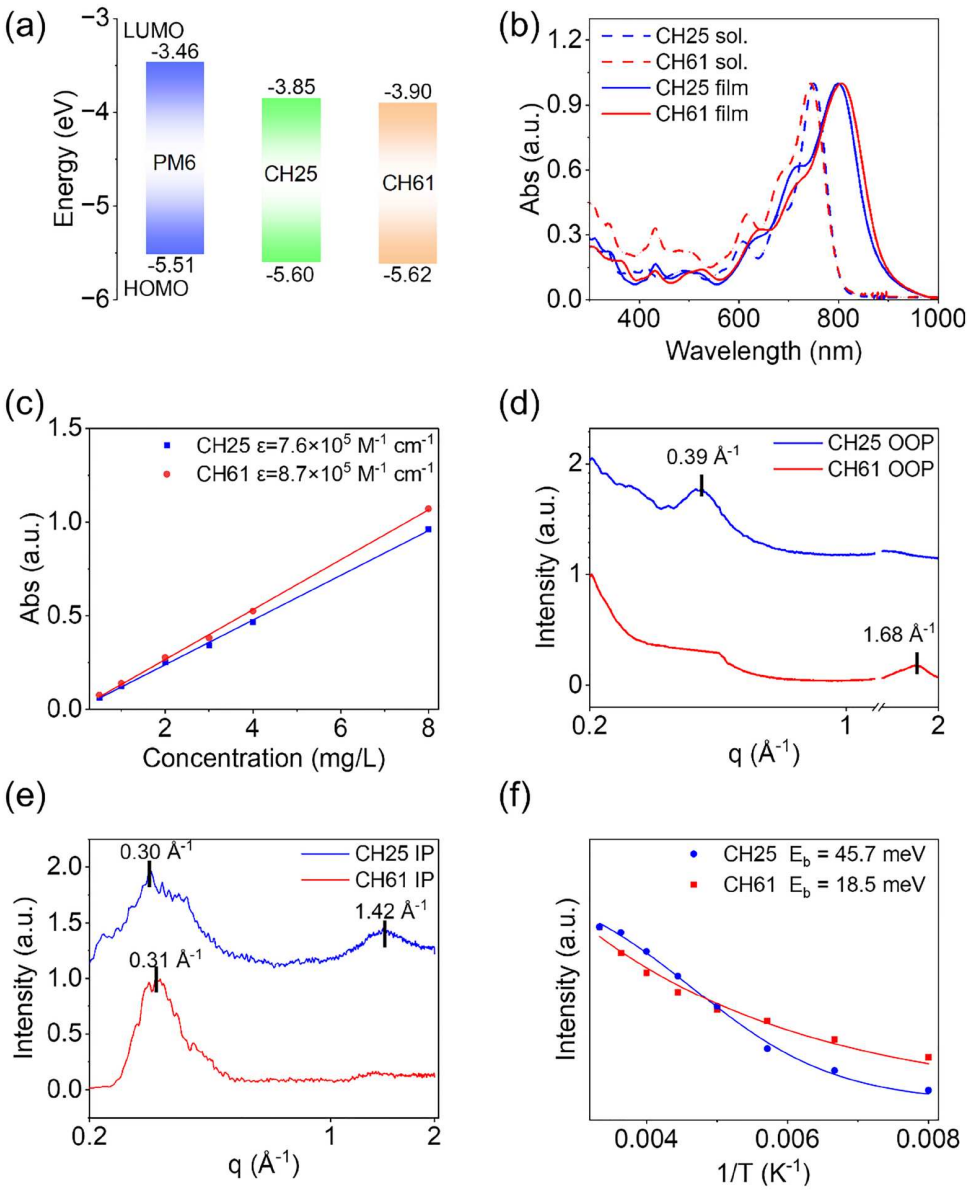

Figure 2 (Color online) (a) Energy level diagram of PM6, CH25, and CH26 films derived from CVs. (b) Absorption spectra in dilute chloroform and solid film. (c) Molar extinction coefficients in dilute chloroform. (d) Out-of-plane line cuts of 2D GIWAXS for pristine films. (e) In-plane line cuts of 2D GIWAXS for pristine films. (f) Exciton binding energies estimated from temperature-dependent PL.

rigid backbone caused by a ring-fusing connection between centrally-extended triptycene and three NFA backbones. On the contrary, despite the similar spatial configuration of CH61, an obvious signal in the OOP direction indicates the markedly π-π stacking between adjacent molecules (Figure S6 and Figure 2d). As the linkages between $Ir(ppy)_3$ moiety and NFA backbone are rotatable C–C single bonds, which will rotate and adjust to specific configurations suitable for intermolecular π-π stackings of CH61 [31,40–42]. Therefore, CH61 yields a π-π stacking distance of 3.74 Å and a large crystal coherence length (CCL) of 21.74 Å (Table S3). In the in-plane (IP) direction, CH61 also displays a stacking distance of 20.3 Å with a much larger CCL of 92.7 Å comparing to 20.9 Å for CH25. Undoubtedly, the better π-π stackings of 3D CH61 will facilitate its efficient charge transport and be beneficial for achieving high-performance OSCs.

As illustrated in Figures S7 and S8, CH61 possesses the smaller Stokes shifts of 38 nm in solution and 60 nm in film comparing to those of 42 and 71 nm for CH25, suggesting the decreased reorganization energy of CH61 that is beneficial for charge transport [43]. The smaller exciton binding energy (E_b) of 18.5 meV for CH61 film could also be observed compared to 45.7 meV for CH25 (Figure 2f), which may be attributed to the larger dipole moment and more delocalized exciton of CH61. A smaller E_b could separate photogenerated excitons of CH61 into free charges under a lower driving force and further reduce the energy losses of OSCs [44–47]. Please note that E_bs were roughly estimated by temperature-dependent photoluminescence (PL) herein. This makes the absolute values of E_b not very meaningful; only the relative magnitude is significant. The exciton lifetimes of two NFAs were similar in both solutions and films (Figures S9 and S10).

To evaluate the photovoltaic performances of CH25 and CH61, the conventional devices were fabricated by using PM6 [48] as the donor material. CH25-based binary OSCs only presented a PCE of 3.41% with a V_{OC} of 0.933 V, J_{SC} of 6.84 mA cm^{-2} and FF of 53.43% (Figure 3a and Table 1). Conversely, CH61-based devices achieved an excellent PCE of 17.85% with a V_{OC} of 0.947 V, J_{SC} of 24.90 mA cm^{-2} and FF of 75.70%, representing a quite rare high-performance system for 3D trimeric acceptors. The significantly

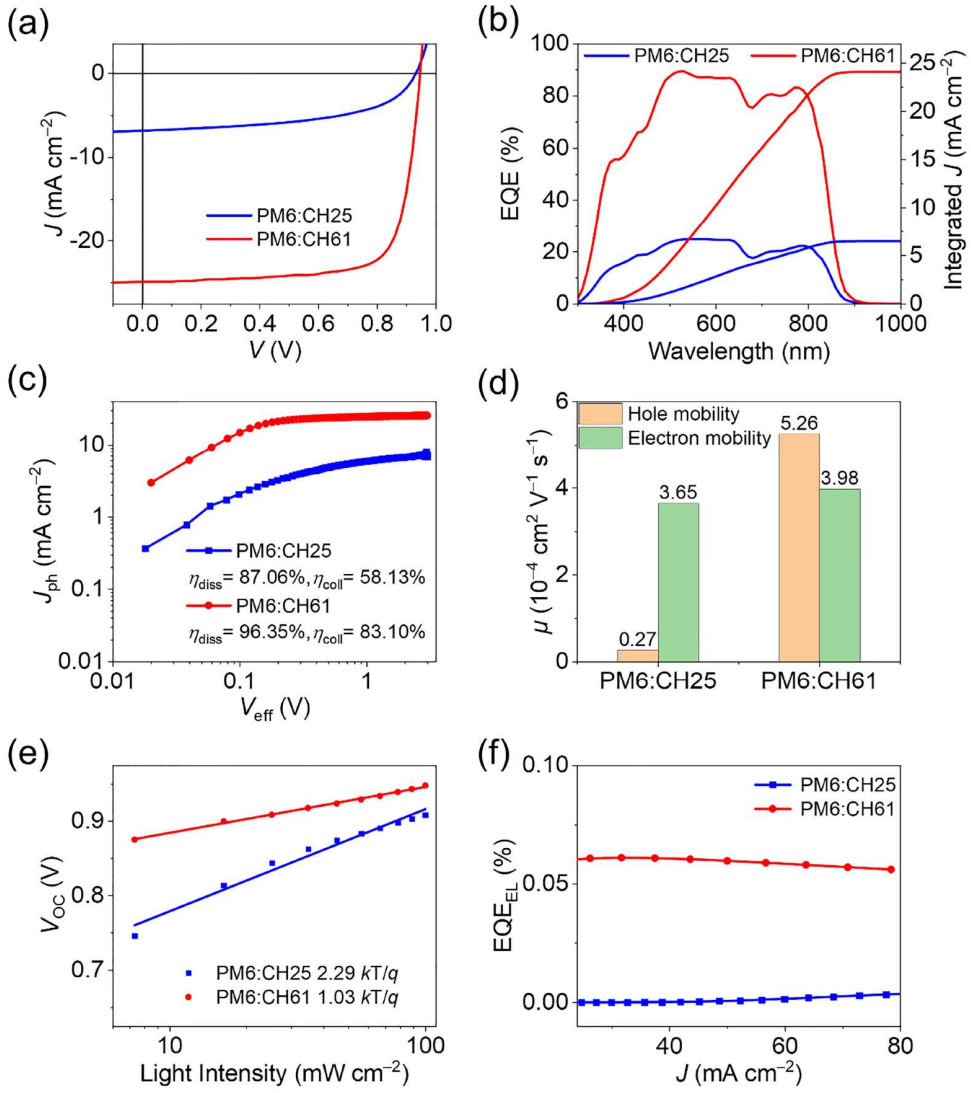

Figure 3 (Color online) (a) Current density-voltage curves. (b) EQE spectra and integral J_{SC}. (c) The dependence of photocurrent density (J_{ph}) *versus* the effective voltage (V_{eff}) curves. (d) Charge carrier mobility of blend films. (e) Light intensity dependence of V_{OC}. (f) EQE_{EL} plots of CH25 and CH61-based devices.

Table 1 Photovoltaic parameters for OSCs[a)]

Active layer	V_{OC} (V)	J_{SC} (mA/cm^2)	$J_{SC}^{b)}$ (mA/cm^2)	FF (%)	PCE (%)
PM6:CH25	0.933 (0.932±0.001)	6.84 (6.68±0.18)	6.50	53.43 (52.58±1.04)	3.41 (3.28±0.15)
PM6:CH61	0.947 (0.945±0.002)	24.90 (24.74±0.09)	24.08	75.70 (75.68±0.22)	17.85 (17.70±0.06)

a) Average parameters derived from 15 independent OSCs (Tables S5 and S6). b) Current densities by integrating EQE plots.

lower external quantum efficiencies (EQEs) of CH25-based devices (Figure 3b) should be attributed to inferior charge transfer/transport dynamics that are closely related to intermolecular packing behaviors and film morphology of CH25. For example, CH25 and CH61-based devices afforded exciton dissociation efficiencies (η_{diss}) of 87.06% and 97.35%; additionally, the charge collection efficiencies (η_{coll}) were estimated as 58.13% and 83.10%, respectively (Figure 3c) [49]. The lower η_{diss} of CH25 is consistent with its quite smaller photoluminescence quenching yield (η_{PLQ}) shown in Figure S12. Moreover, the PM6:CH61-based device shows the larger and more balanced hole/electron mobility (Figure 3d and Figure S13), which should contribute a lot to its better charge transport and collection [50,51]. In sharp contrast to PM6:CH25, the bimolecular recombination in PM6:CH61 is significantly suppressed, as indicated by a slope close to kT/q (Figure 3e) [52]. A detailed energy loss (E_{loss}) analysis afforded the total E_{loss} of 0.533 and 0.524 eV for CH25- and CH61-based devices, respectively (Figure S14 and Table S4). It is worth noting that the non-radiative energy loss (ΔE_3) of the PM6:CH61-based device is significantly smaller than that of PM6:CH25, indicated by the markedly large electroluminescence/fluorescence quantum yields (Figure 3f and Figure S15). A key advantage of 3D-shaped acceptors is their ability to effectively suppress the aggregation-caused quenching (ACQ) effect of acceptor molecules, thereby enabling high quantum yields and minimal non-radiative energy losses in the solid state [53,54]. The obvious J-aggregation and suppressed H-aggregation of CH61 may account for the higher fluorescence quantum yield [53]. Besides, the PM6:CH61-based device exhibited a smaller Urbach

energy of approximately 23.4 meV than PM6:CH25 based one (25.2 meV, Figure S16), further revealing the low energy disorder in PM6:CH61 films [55].

To gain further insights into the significantly enhanced PCE for PM6:CH61-based devices, we employed femtosecond transient absorption (fs-TA) spectroscopy to probe the photo-induced charge transfer dynamics. As illustrated in Figure 4a, b, the significant difference is the lack of the donor's ground-state bleaching (GSB) signal at 630 nm [56,57], in PM6:CH25 blend films, while it is apparent in PM6:CH61 blends [58]. This demonstrates the ineffective hole transfer at the donor/acceptor interface for PM6:CH25, which consists well with the quite small hole mobility and poor PCEs. As revealed in Figure 4c and Figure S17, the PM6:CH25-based active layer exhibited an extremely rough surface with a root-mean-square (RMS) value of 15.74 nm, likely due to the highly rigid backbone and 3D spatial configuration of CH25. Besides, the quite poorer solubility of CH25 and its bad miscibility with PM6 (Figure S18 and Table S7) should also be responsible for the large RMS of CH25-based films, and further limit the improvement of resulting OSCs. On the contrary, PM6:CH61-based films exhibited a smoother and more uniform surface with the RMS value of 0.92 nm. Moreover, the suitable donor/acceptor phase separation is also observed in PM6:CH61 blend films, but not in PM6:CH25 (Figure 4d). In PM6:CH25 blended films, a similar molecular packing behavior as CH25 neat films was exhibited (Figure 4e, f), as the π-π stacking in the OOP direction was apparently weak even with the facilitation of PM6. In sharp contrast, the diffraction in the OOP direction for PM6:CH61 was easily noticed with a π-π stacking distance of 3.88 Å and a relatively large CCL of 22.90 Å. The irregular packing of CH25 and poor film morphology should be responsible for the significantly inferior charge transfer/transport and photovoltaic performance.

3 Conclusions

With the aim of combining the advantages of fullerene and NFAs, we proposed a new molecular design pathway of building fullerene-conformation-mimicking NFAs: extending the backbone of NFAs through a 3D molecular centrally-extended center. Herein, two 3D centrally-extended cores of triptycene and octahedral chelated iridium(III) complex were employed, affording the three-dimensional trimeric NFAs of CH25 and CH61 after extending six cantilevers towards different directions. Compared to the highly rigid and symmetrical CH25, CH61 gives a relatively flexible molecular skeleton caused by the featured coordinate bond and single-bond connection between the iridium(III) complex and NFA backbones. A systematic investigation disclosed that both CH25 and CH61 exhibit the propeller-like fullerene-mimicking conformations; however, their different skeleton rigidity and conjugated orientation cause quite different intermolecular stacking behavior and nanos-

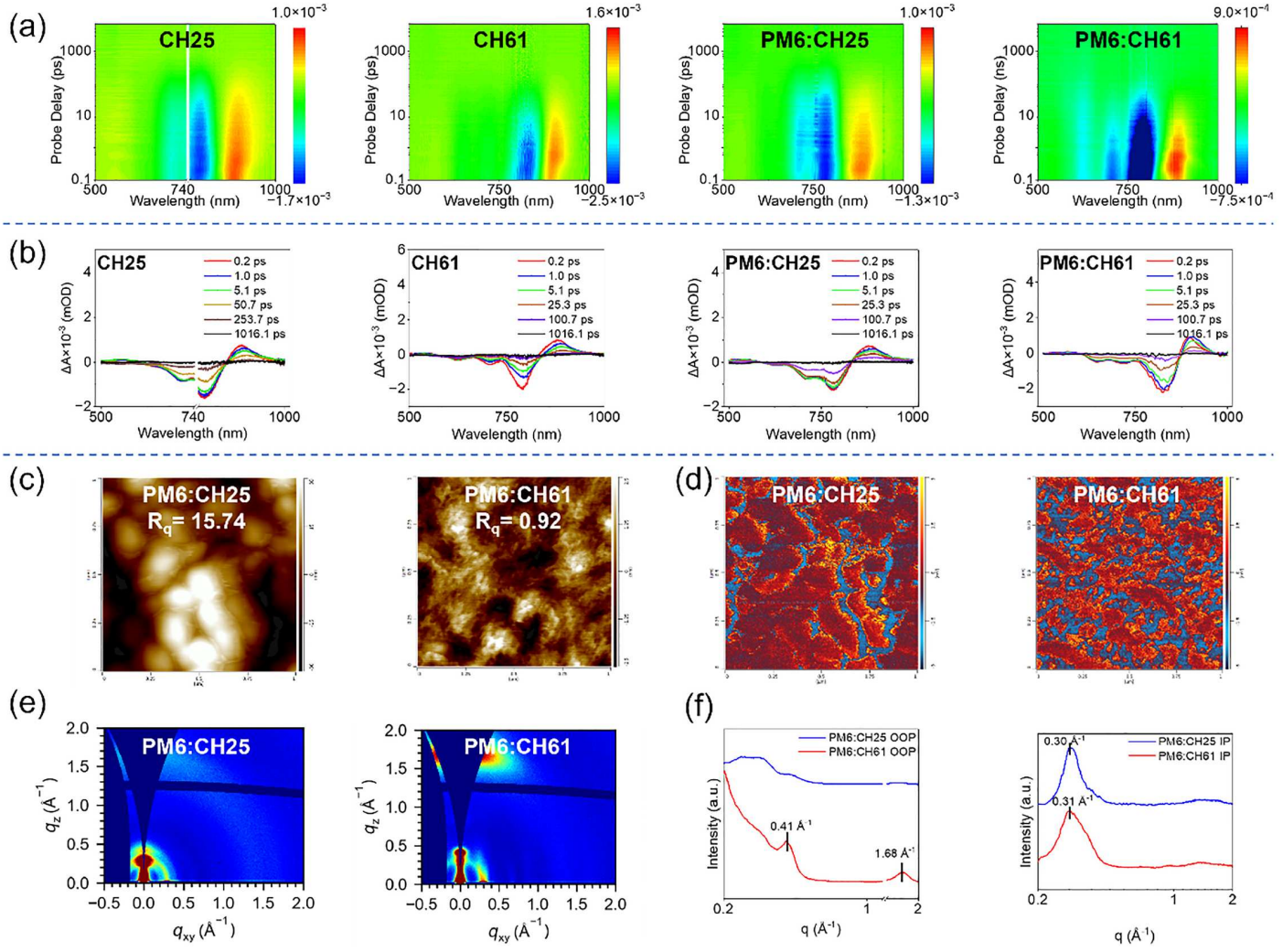

Figure 4 (Color online) (a) Contour plots of the TAS spectra of neat and blend films excited at 762 nm. (b) TAS spectra of neat and blend films at different delay times. (c) AFM height image of blended films. (d) AFM-IR image of blended films. (e) 2D GIWAXS patterns of blended films. (f) OOP and IP line cuts of 2D GIWAXS for blended films.

cale film morphology. The more favorable aggregation of CH61 gives rise to the weaker exciton binding, more balanced hole/electron transport and suppressed non-radiative recombination. Finally, PM6:CH61-based binary OSC achieves an excellent efficiency of 17.85%, which not only greatly surpasses that of 3.41% for PM6:CH25 but also represents a quite rare high-performance system for 3D trimeric acceptors. By presenting such a design vision of fullerene-mimicking, our work will inspire further efforts to explore highly efficient fullerene-like NFAs with a two-in-one feature of both fullerene and NFAs.

Conflict of interest

The authors declare no conflict of interest.

Acknowledgement

This work was supported by the Ministry of Science and Technology of China (National Key R&D Program of China) (2022YFB4200400), the National Natural Science Foundation of China (22479081, 22309090, 52025033, 22361132530, 52373189), the Natural Science Foundation of Tianjin (23JCZDJC01160) and the Haihe Laboratory of Sustainable Chemical Transformations.

Supporting information

The supporting information is available online at http://chem.scichina.com and http://link.springer.com/journal/11426. The supporting materials are published as submitted, without typesetting or editing. The responsibility for scientific accuracy and content remains entirely with the authors.

References

1 Chang Y, Zhang J, Chen Y, Chai G, Xu X, Yu L, Ma R, Yu H, Liu T, Liu P, Peng Q, Yan H. *Adv Energy Mater*, 2021, 11: e2100079
2 Yan P, Yang D, Wang H, Yang S, Ge Z. *Energy Environ Sci*, 2022, 15: 3630–3669
3 Wei W, Yuan X, Zhou X, Li Y, Lee S, Xu J, Zhang Y, Feng H, Jiang Q, Wu J, Yang C, Hao X, Huang F, Cao Y, Duan C. *Angew Chem Int Ed*, 2025, 64: e202517485
4 Yi L, Dai S, Sun R, Wang W, Wu Y, Jiao X, Zhang C, Min J. *Org Electron*, 2020, 87: 105963
5 Shi H, Fu W, Shi M, Ling J, Chen H. *J Mater Chem A*, 2015, 3: 1902–1905
6 Fan J, Liu Z, Chen H, Li C. *Adv Mater*, 2025, 37: 2419525
7 You Z, Wen J, Liu W, Fink Z, Wu X, Seong H, Wang Y, Zhang L, Wang X, Russell TP, Liu Y. *Adv Mater*, 2025, 37: 2500450
8 Xiao Z, Li S, Liu J, Chen X, Suo Z, Li C, Wan X, Chen Y. *Sol RRL*, 2024, 8: 2400206
9 Ye Q, Song W, Bai Y, Chen Z, Ding P, Ge J, Meng Y, Han B, Zhou X, Ge Z. *Energy Environ Sci*, 2025, 18: 4373–4383
10 Ganesamoorthy R, Sathiyan G, Sakthivel P. *Sol Energy Mater Sol Cells*, 2017, 161: 102–148
11 Scharber MC. *Adv Mater*, 2016, 28: 1994–2001
12 Liu T, Troisi A. *Adv Mater*, 2013, 25: 1038–1041
13 Zhang C, Langner S, Mumyatov AV, Anokhin DV, Min J, Perea JD, Gerasimov KL, Osvet A, Ivanov DA, Troshin P, Li N, Brabec CJ. *J Mater Chem A*, 2017, 5: 17570–17579
14 Ko S, Lee W, Choi H, Walker B, Yum S, Kim S, Shin TJ, Woo HY, Kim JY. *Adv Energy Mater*, 2015, 5: 1401687
15 Hou J, Inganäs O, Friend RH, Gao F. *Nat Mater*, 2018, 17: 119–128
16 Shi K, Liu H, Qin S, Zhao Q, Mou X, Liang J, Yao J, Zhu C, Zhong L, Guo J, Zhang J, Wu Y, Zhang Z, Qiu B, Li Y. *Angew Chem Int Ed*, 2025, 64: e202514004
17 Wang R, Si X, Mei L, Zhao W, Shi W, Chen XK, Song G, Li L, Xiao Z, Yao Z, Long G, Li C, Wan X, Chen Y. *J Am Chem Soc*, 2025, 147: 43629–43639
18 Yin K, Li Y, Li X, He H, Gong Y, Qin S, Yuan M, Chen Z, Zhang J, Zhang J, Wei Z, Meng L, Li Y. *ACS Energy Lett*, 2025, 10: 6004–6013
19 Gao C, Wang Y, Tian H, Sun K, Zhao C, Che J, Qiu S, Chen W, Huang C, Wang Z, Hu H, Han P, Li S, Luo Z, Zhang G. *Adv Mater*, 2026, 38: e17576
20 Zhao B, Zhu L, Xiong S, Yu J, Wang X, Zhao J, Tan L, Zhang J, Zhong J, Kan L, Wan X, Jiang K, Li H, Ma Z, Liu Y, Zhu H, Kan Z, Liu F, Sun Z, Chu J, Bao Q. *Adv Energy Mater*, 2025, 15: e04947
21 Yao Z, Wan X, Li C, Chen Y. *Acc Mater Res*, 2023, 4: 772–785
22 Ma R, Luo Z, Zhang Y, Zhan L, Jia T, Cheng P, Yan C, Fan Q, Liu S, Ye L, Zhang G, Xu X, Gao W, Wu Y, Wu J, Li Y, Liu Y, Liu F, Song J, Chen H, Chen W, Zhang X, Liu Y, Yuan J, Liu Q, Kan Z, Yin H, Li X, Ma Y, Deng D, Zhu L, Huo Y, Fan B, Fu H, Liao X, Hu H, Li C, Yu R, Hu H, Yao Z, Cai Y, Qian D, Cui Y, Yao H, Xu B, Kan B, Gao K, Duan C, Hu X, Sun H. *Sci China Mater*, 2025, 68: 1689–1701
23 Li CZ, Chueh CC, Yip HL, Zou J, Chen WC, Jen AKY. *J Mater Chem*, 2012, 22: 14976–14981
24 Zhou H, Liu C, Liu S, Zhang Z, Sun S, Xu W, Ma X, Wang J, Xu Y, Du X, Jeong SY, Woo HY, Zhang F, Sun Q. *Small*, 2024, 20: 2308216
25 Fang H, Chen Q, Lin Y, Xu X, Wang J, Li M, Xiao C, McNeill CR, Tang Z, Lu Z, Li W. *Angew Chem Int Ed*, 2025, 64: e202417951
26 Liu Y, Mu C, Jiang K, Zhao J, Li Y, Zhang L, Li Z, Lai JYL, Hu H, Ma T, Hu R, Yu D, Huang X, Tang BZ, Yan H. *Adv Mater*, 2015, 27: 1015–1020
27 Lee J, Singh R, Sin DH, Kim HG, Song KC, Cho K. *Adv Mater*, 2016, 28: 69–76
28 Liu X, Cai Y, Huang X, Zhang R, Sun X. *J Mater Chem C*, 2017, 5: 3188–3194
29 Yang T, Wang B, He Y, Zhou A, Yao Z, Xing G, Tao Y. *Inorg Chem*, 2023, 62: 5920–5930
30 Yang T, Gao X, He Y, Wang H, Tao Y. *J Mater Chem C*, 2020, 8: 5761–5768
31 Chen H, Zhang Z, Wang P, Zhang Y, Ma K, Lin Y, Duan T, He T, Ma Z, Long G, Li C, Kan B, Yao Z, Wan X, Chen Y. *Energy Environ Sci*, 2023, 16: 1773–1782
32 Li Y, Ge Z, Mei L, Ma H, Chen Y, Wang X, Yu J, Lu G, Yang R, Chen X, Yin S, Sun Y. *Angew Chem Int Ed*, 2024, 63: e202411044
33 Qi F, Li Y, Zhang R, Lin FR, Liu K, Fan Q, Jen AK. *Angew Chem Int Ed*, 2023, 62: e202303066
34 Chang B, Zhang Y, Zhang C, Zhang M, Wang Q, Xu Z, Chen Q, Bai Y, Fu H, Meng S, Xue L, Kim S, Yang C, Yi Y, Zhang Z. *Angew Chem Int Ed*, 2024, 63: e202400590
35 Lee J, Sun C, Lee J, Kim DJ, Kang WJ, Lee S, Kim D, Park J, Phan TN, Tan Z, Kim FS, Lee J, Bao X, Kim T, Kim Y, Kim BJ. *Adv Energy Mater*, 2024, 14: 2303872
36 Xu Z, Li S, Huang F, He T, Jia X, Liang H, Guo Y, Long G, Kan B, Yao Z, Li C, Wan X, Chen Y. *Angew Chem Int Ed*, 2023, 62: e202311686
37 Wu BH, Huang MJ, Lai CC, Cheng CH, Chen IC. *Inorg Chem*, 2018, 57: 4448–4455
38 Zhao Q, He F. *J Energy Chem*, 2024, 93: 174–192
39 Zhao Q, Lai H, Chen H, Li H, He F. *J Mater Chem A*, 2021, 9: 1119–1126
40 Wang J, Wang P, Chen T, Zhao W, Wang J, Lan B, Feng W, Liu H, Liu Y, Wan X, Long G, Kan B, Chen Y. *Angew Chem Int Ed*, 2025, 64: e202423562
41 Cui T, Huang Z, Zhang Y, Ru XP, Bi X, Ding YT, Yang Y, Dai J, Lu G, Liu Z, Chen Y, Zhang HL. *J Mater Chem A*, 2024, 12: 6996–7004
42 Ran X, Qiu D, Shi Y, Zhang H, Zhang J, Wei Z, Lu K. *Chem Commun*, 2024, 60: 10548–10551
43 Xiao Y, Cui Y, Yuan H, Wang J, Chen Z, Wang GL, Fu W, Fu Z, Wang Y, Zhang T, Yu Y, Yu R, Zuo G, Zhang M, Hao X, Hou J. *Energy Environ Sci*, 2025, 18: 7136–7145
44 Dong J, Li Y, Liao C, Xu X, Yu L, Li R, Peng Q. *Energy Environ Sci*, 2025, 18: 4982–4995
45 Zhu L, Huang M, Han G, Wei Z, Yi Y. *Angew Chem Int Ed*, 2025, 64: e202413913
46 Leblebici SY, Chen TL, Olalde-Velasco P, Yang W, Ma B. *ACS Appl Mater Interfaces*, 2013, 5: 10105–10110
47 Guo Y, Han G, Guo J, Guo H, Fu Y, Miao X, Wang Z, Li D, Li S, Xu X, Lu X, Chen H, Yi Y, Chow PCY. *Energy Environ Sci*, 2024, 17: 8776–8786
48 Zhang M, Guo X, Ma W, Ade H, Hou J. *Adv Mater*, 2015, 27: 4655–4660
49 Koster LJA, Kemerink M, Wienk MM, Maturová K, Janssen RAJ. *Adv Mater*, 2011, 23: 1670–1674
50 Zhang F, Yin Y, Li M, Liu Y, Jiang J, Li X. *Adv Funct Mater*, 2024, 34: 2406066
51 Liao X, Liu M, Pei H, Zhu P, Xia X, Chen Z, Zhang Y, Wu Z, Cui Y, Xu G, Gao M, Ye L, Ma R, Liu T, Lu X, Zhu H, Chen Y. *Angew Chem Int Ed*, 2024, 63: e202318595
52 Zeiske S, Sandberg OJ, Zarrabi N, Li W, Meredith P, Armin A. *Nat Commun*, 2021, 12: 7
53 Lu H, Li D, Liu W, Ran G, Wu H, Wei N, Tang Z, Liu Y, Zhang W, Bo Z. *Angew Chem Int Ed*, 2024, 63: e202407007
54 Zhu X, Gu C, Cheng Y, Lu H, Wang X, Ran G, Zhang W, Tang Z, Bo Z, Liu Y. *Adv Mater*, 2025, 37: 2507529
55 Zhang Z, Li Y, Cai G, Zhang Y, Lu X, Lin Y. *J Am Chem Soc*, 2020, 142: 18741–18745
56 Pananusorn P, Sotome H, Uratani H, Ishiwari F, Phomphrai K, Saeki A. *J Chem Phys*, 2024, 161: 184710
57 Shen Q, He C, Li S, Qiao J, Li S, Zhang Y, Shi M, Zuo L, Hao X, Chen H. *Small*, 2024, 20: 2403570
58 Liu X, Zhang Z, Wang C, Zhang C, Liang S, Fang H, Wang B, Tang Z, Xiao C, Li W. *Angew Chem Int Ed*, 2024, 63: e202316039